Doping mechanism in pure CuInSe2

F. Werner, D. Colombara, M. Melchiorre, N. Valle, B. El Adib, C. Spindler, and S. Siebentritt

---

Articles you may be interested in

Electrical properties from photoinduced charging on Cd-doped (100) surfaces of CuInSe2 epitaxial thin films
J. Vac. Sci. Technol. A **34**, 031201 (2016); 10.1116/1.4945105

Chemical reactions at CdS heterojunctions with CuInSe2
J. Vac. Sci. Technol. A **31**, 021202 (2013); 10.1116/1.4775341

Growth and characterization of iron-doped semi-insulating InP buffer layers for Al-free GaInP/GaInAs high electron mobility transistors
J. Appl. Phys. **108**, 114502 (2010); 10.1063/1.3516490

Si diffusion in p- GaN
J. Vac. Sci. Technol. B **22**, 1727 (2004); 10.1116/1.1767826

Diffusion of zinc acceptors in InAsP by the metal-organic vapor-phase diffusion technique
Appl. Phys. Lett. **71**, 900 (1997); 10.1063/1.119682

Doping mechanism in pure CuInSe$_2$

F. Werner,[1] D. Colombara,[1] M. Melchiorre,[1] N. Valle,[2] B. El Adib,[2] C. Spindler,[1]
and S. Siebentritt[1]

[1]*Physics and Materials Science Research Unit, University of Luxembourg, Rue du Brill 41,
L-4422 Belvaux, Luxembourg*
[2]*Materials Research and Technology Department, Luxembourg Institute of Science and Technology,
Rue du Brill 41, L-4422 Belvaux, Luxembourg*

We investigate the dopant concentration and majority carrier mobility in epitaxial CuInSe$_2$ thin films for different copper-to-indium ratios and selenium excess during growth. We find that all copper-poor samples are *n*-type, and that hopping conduction in a shallow donor state plays a significant role for carrier transport. Annealing in sodium ambient enhances gallium in-diffusion from the substrate wafer and changes the net doping of the previously *n*-type samples to *p*-type. We suggest that sodium incorporation from the glass might be responsible for the observed *p*-type doping in polycrystalline Cu-poor CuInSe$_2$ solar cell absorbers. *Published by AIP Publishing.*
[http://dx.doi.org/10.1063/1.4947585]

I. INTRODUCTION

In the ternary chalcopyrite semiconductors CuInSe$_2$ and CuGaSe$_2$ and their alloy Cu(In,Ga)Se$_2$, applied as absorbers in thin film photovoltaic devices, a large number of intrinsic point defect species exist due to the presence of 3 or 4 distinct atomic species.[1] As a consequence, chalcopyrite absorbers are typically highly compensated and their electrical properties are dominated by intrinsic defects rather than extrinsic dopants. For the fabrication of optimized highly efficient solar cell absorbers, however, precise control over the carrier polarity (*n*-type or *p*-type doping) and the net dopant concentration is indispensable.

Although many studies in previous decades have focused on the electrical properties of CuInSe$_2$ grown with carefully controlled chemical composition, most were performed on stoichiometric material. With respect to non-stoichiometry, earlier studies only agree that nominally Cu-rich CuInSe$_2$ (Cu:In > 1 during the growth process) grown or annealed under Se excess is always *p*-type, while for all other combinations of Cu and Se conditions both *n*- and *p*-type samples are reported by different authors.[2–7] Furthermore, the net doping in *p*-type samples was found to decrease with lower Cu:In ratios.[2,6] However, the highly *p*-conducting copper selenide secondary phase observed under Cu-rich growth conditions had not been etched in these studies, and hence will be at least partly responsible for the observed *p*-type doping of Cu-rich samples.

Cu-poor polycrystalline Cu(In,Ga)Se$_2$ solar cell absorbers grown on glass, on the other hand, are always *p*-type. Particularly, the *p/n*-junction in chalcopyrite thin film solar cells works on the assumption of a strongly *n*-doped window layer and a *p*-type absorber. The *p*-type conductivity of typical solar cell absorbers might be related to a pronounced Se excess during absorber deposition,[8,9] but also diffusion of impurities from the glass substrates cannot be excluded. Furthermore, Na treatment of Cu(In,Ga)Se$_2$ absorbers is known to increase the net *p*-type doping,[10–15] and accordingly the carrier polarity of Cu-poor CuInSe$_2$ might be sensitive to trace amounts of Na in the films. Although less relevant for the study of pure CuInSe$_2$, it is worth noting that pure CuGaSe$_2$ is always found to be *p*-type in any composition,[16,17] and hence replacing In by Ga appears to favor *p*-type doping.

In this contribution we aim to address the electronic properties of only the CuInSe$_2$ without grain boundaries, contaminations, or any intentional doping by extrinsic impurities. In the following we refer to this as pure CuInSe$_2$. We study Cu-poor epitaxial thin films of pure grown under a variation of the Se excess and copper-to-indium supply during growth. We also investigate the effect of extrinsic sodium doping via the gas phase on the conductivity type of the CuInSe$_2$ films free from grain boundaries.

II. ABSORBER GROWTH AND CHEMICAL COMPOSITION

Epitaxial CuInSe$_2$ films with a thickness of 800–1200 nm were grown by metal-organic vapor phase epitaxy (MOVPE) on (100)-oriented semi-insulating monocrystalline GaAs substrate wafers with a thickness of 500 μm. The substrate temperature was set to 470 °C for all samples. Cyclopentadienyl-copper-triethyl phosphine (CpCuTEP), trimethyl-indium (TMI), and ditertiarybutyl selenide (DtBSe) in a flow of hydrogen gas are used as precursors. The chemical composition of the CuInSe$_2$ films is controlled by varying the TMI and DtBSe partial pressures (denoted in the following as p_{In} and p_{Se}), while the CpCuTEP partial pressure is kept constant at $p_{Cu} = 0.45$ mbar. A balancing flow of hydrogen in each delivery line ensures that the total gas flow and the reactor pressure of 50 mbar are constant for all depositions. The samples analyzed in this study cover a range of partial pressure ratios of $p_{Cu}/p_{In} = 0.6$–1.2 and $p_{Se}/(p_{Cu} + p_{In}) = 22$–32. Such pronounced Se excess is necessary in order to obtain a kinetically limited epitaxial growth mode at the chosen growth temperature and a good crystal quality.[18]

We determine the chemical composition of the semiconductor layers by energy-dispersive X-ray (EDX) analysis in a scanning electron microscope (SEM) at an accelerating voltage of 10 kV. Note, that no post-growth chemical etching was applied before the EDX study in order to detect the total amount of copper and selenium present, independent of chemical phase. However, as expected, only the most Cu-rich sample shows evidence of a copper selenide film partially covering the surface. This starting formation of a secondary phase indicates a chemical composition close to stoichiometry. Although absolute values of atomic concentrations are difficult to obtain reliably from EDX measurements, relative trends between similar samples are reliable and we use EDX spectra recorded away from the Cu_xSe phase on the most Cu-rich sample to scale the atomic ratios obtained by the EDX analysis to yield the expected ratio of $Cu:In:Se = 1:1:2$ near stoichiometry.

Figure 1 shows the resulting selenium-to-metal [Se:(Cu + In)] and copper-to-indium (Cu:In) atomic ratios determined by EDX as a function of the ratio of the precursor partial pressures (p_{Cu}/p_{In}, calculated from the specified precursor flows) for different selenium supplies given by the precursor partial pressure ratio $p_{Se}/(p_{Cu} + p_{In})$. The error bars represent the spread in values determined at three different spots on the sample, not taking into account the uncertainties in the EDX analysis.

For medium selenium supply [$p_{Se}/(p_{Cu} + p_{In}) = 26$, red circles in Fig. 1] the Cu:In atomic ratio first increases linearly with increasing precursor pressure ratio p_{Cu}/p_{In}, and then saturates near stoichiometry for $p_{Cu}/p_{In} > 0.75$. For higher selenium supply the copper incorporation into the growing absorber film appears to be hindered, and significantly lower Cu:In ratios are observed for comparable ratios of p_{Cu}/p_{In}. As the EDX analysis is performed without KCN etching, the reduced copper content in the absorber film cannot be attributed to the formation of a surface phase, e.g., Cu_xSe, as this phase would contribute to the EDX signal as

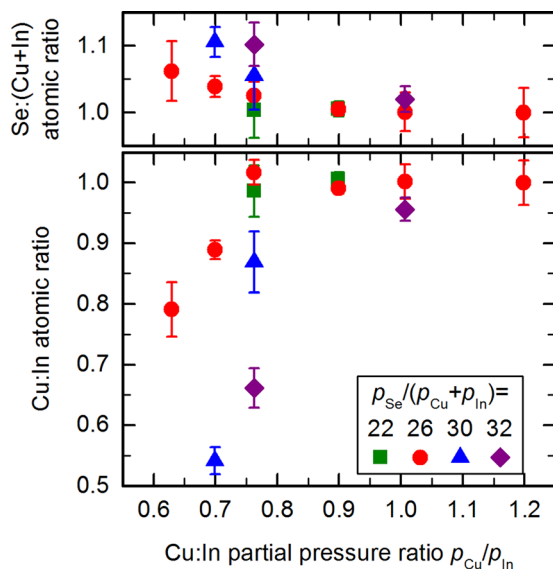well. However, the reduced copper content of the films might indicate a parasitic precursor reaction upstream of the sample in the growth reactor.

Due to the suppressed copper incorporation for high selenium supply, we obtain Cu:In ratios as low as 0.5, which corresponds to only 16 at. % copper. According to the pseudo-binary phase diagram of $CuInSe_2$ along the In_2Se_3-Cu_2Se sub-system,[19] the samples analyzed in this study cover the transition from a pure chalcopyrite phase via a chalcopyrite/defect mixed phase to a pure defect phase. Due to the systematic uncertainty in the EDX analysis, however, an unambiguous assignment of specific absorbers to the different phases is not always possible. In the following, we assign all samples with Cu:In > 0.8 to the chalcopyrite phase, but considerable uncertainty remains for those absorbers close to the transition region.

III. ELECTRONIC PROPERTIES OF PURE Cu-POOR CuInSe$_2$

We determine the majority carrier concentration and Hall mobility by Hall measurements in the van der Pauw configuration[20] under varying magnetic fields. For the fabrication of Hall specimen, all the samples were etched for 3 min in a 10% solution of KCN in order to clean the surface to achieve better ohmic contacts, and to make sure no secondary copper selenide phases are present. Triangular gold contacts (contact area 0.5–1.5 mm^2) with a thickness of 300 nm were defined on the corners of 5 × 5 mm^2 pieces of the sample by electron beam evaporation through a shadow mask for contacting with conductive silver paste. Thermally conductive glue was used to ensure a good thermal contact between the specimen and the copper sample holder of the Hall setup.

Hall effect measurements were carried out in magnetic fields of up to 9 T using a superconducting magnet in a closed-cycle cryostat. We apply the correction factors for finite contact size according to Chwang *et al.*[21] The Hall scattering factor r is assumed to be unity. For selected samples the temperature-dependent carrier density and mobility are measured by slowly cooling down the sample in the cryostat. For all other measurements the sample temperature is set to 270 K in order to ensure optimal cooling of the superconducting magnet, which allows significantly shorter measurement times compared with room temperature. Furthermore, temperature-dependent measurements indicate only a small change in the carrier density below 10% in this temperature range. The sample temperature is measured at the back of the sample holder and is calibrated to be correct within ±1 K. Cross-sectional SEM images and *in-situ* reflectometry measurements were used to determine the thickness of the absorber films, in order to calculate the bulk carrier densities from the measured sheet carrier densities. For all the samples, the absorber thickness is between 800 and 1200 nm.

The majority carrier type is determined from the polarity of the Hall voltage. Only one sample with the highest copper-to-indium partial pressure ratio shows hole conductivity (*p*-type); all other samples show electron conductivity (*n*-type). Hence in pure Cu-poor CuInSe$_2$, independent of Se supply, we cannot reproduce the *p*-type polarity commonly observed for polycrystalline Cu-poor thin film solar

FIG. 1. Selenium-to-metal atomic ratio Se:(Cu + In) (top) and copper-to-indium atomic ratio Cu:In (bottom) determined by EDX as a function of the precursor partial pressure ratio p_{Cu}/p_{In} for different selenium supplies.

cell absorbers. We will address this conundrum in more detail in Sec. V.

Figure 2 shows the majority carrier (electron) density n for all n-type samples as a function of the atomic Cu:In ratio [Fig. 2(a)] and the ratio p_{Cu}/p_{In} of partial pressures [Fig. 2(b)], respectively. It is apparent that samples with the highest Cu deficiency (lowest Cu:In), expected to contain predominantly a defect phase, are highly n-doped with electron concentrations well above $10^{17}\,cm^{-3}$. For the chalcopyrite films, several trends of the electron concentration can be deduced from Fig. 2:

- For significantly Cu-poor films the electron density appears to decrease for higher Cu:In atomic ratios in the films. Near stoichiometry (Cu:In ≈ 1) the electron density decreases with higher Cu supply, given by the partial pressure ratio p_{Cu}/p_{In}, although the actual Cu incorporation into these films is nearly identical.
- A variation of the selenium supply in the range of $p_{Se}/(p_{Cu}+p_{In})=22$–$32$ investigated here results in electron densities which differ by as much as one order of magnitude. However, for a given Cu supply the absorber grown with $p_{Se}/(p_{Cu}+p_{In})=26$, which is the standard value used in our laboratory to deposit epitaxial CuInSe$_2$ films, always yields the lowest net dopant concentration.

From these observations we conclude that the carrier polarity (n- or p-doping) of the Cu-poor CuInSe$_2$ thin films is
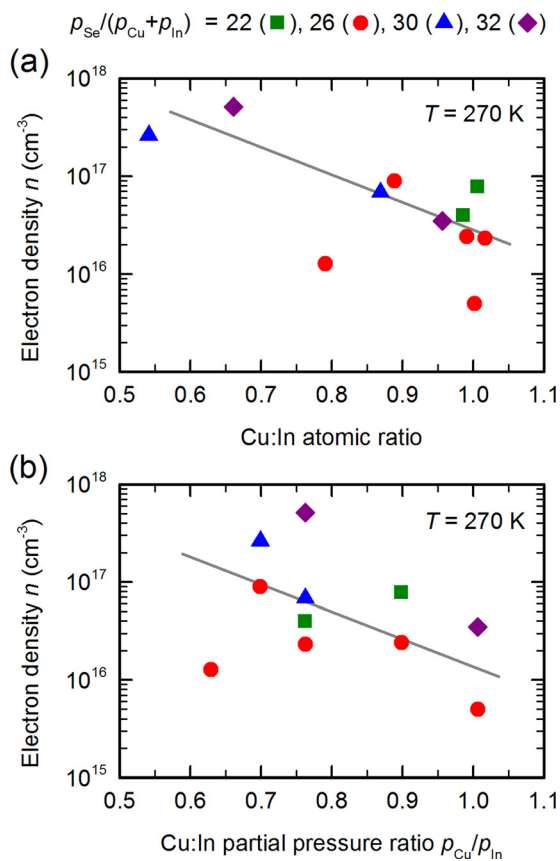

$p_{Se}/(p_{Cu}+p_{In})$ = 22 (■), 26 (●), 30 (▲), 32 (◆)

FIG. 2. Electron concentration n determined by Hall effect measurements at a sample temperature of $T=270\,K$ as a function of (a) the Cu:In atomic ratio and (b) the precursor partial pressure ratio p_{Cu}/p_{In} for different selenium supplies. Gray lines are guides to the eye.

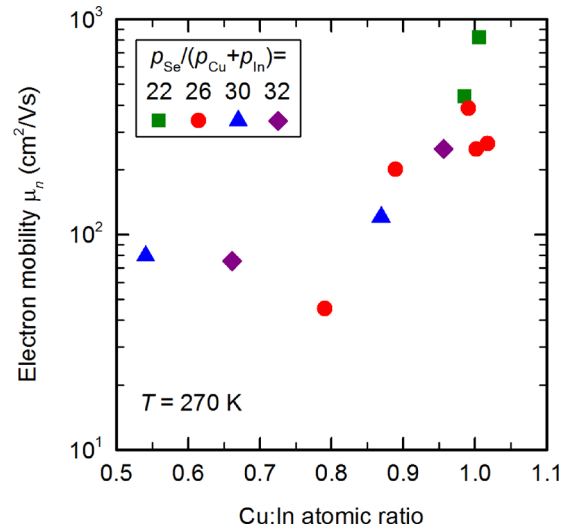FIG. 3. Electron mobility μ_n determined by Hall effect measurements at a sample temperature of $T=270\,K$ as a function of the Cu:In atomic ratio for different selenium supplies.

not related to the amount of selenium excess in the range investigated here. Correspondingly, the net doping is mainly determined by the Cu excess (or deficiency) in the growth process, here given by the partial pressure ratio, and p-type doping is only observed for Cu-rich growth conditions.

Figure 3 shows the electron mobility μ_n as a function of the atomic Cu:In ratio. For the samples dominated by the defect phase (Cu:In < 0.8) we obtain a constant electron mobility of $\mu_n = 75$–$80\,cm^2/Vs$. For the chalcopyrite absorbers the electron mobility increases with higher Cu:In ratio, consistent with the expected lower density of scattering defect centers for compositions closer to stoichiometry. For the nearly stoichiometric samples (and accordingly highest mobility values) we observe a pronounced variation of the electron mobility. While the electron mobility seems to saturate at a value of $\mu_n = 200$–$300\,cm^2/Vs$ for moderate and high selenium supply, significantly higher values of up to $\mu_n = 820\,cm^2/Vs$ are achieved for the lowest selenium supply of $p_{Se}/(p_{Cu}+p_{In})=22$. The improved electron mobility correlates with a change in surface morphology under the influence of a low selenium partial pressure. Figure 4 shows top-view scanning electron microscope (SEM) images of absorber films grown under low $[p_{Se}/(p_{Cu}+p_{In})=22$, Fig. 4(a)] and moderate $[p_{Se}/(p_{Cu}+p_{In})=26$, Fig. 4(b)] selenium supply, respectively. Figure 4(b) is also representative
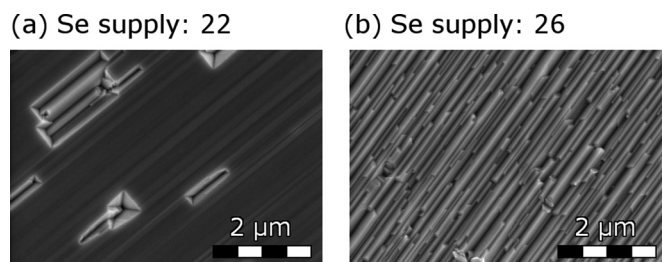

FIG. 4. Top-view scanning electron microscope images of nearly stoichiometric absorbers grown under different selenium supplies with $p_{Se}/(p_{Cu}+p_{In})=22$ (a) and 26 (b), respectively.

for higher selenium partial pressures. Cross-sectional SEM images indicate smooth single crystals in both cases, and thus it is likely that the structures observed in Fig. 4 are related to different preferred surface orientations at different Se fluxes. Accordingly, we attribute the wide spread of mobility values for different selenium supplies to the different impact of surface scattering on the effective mobility.

IV. DEFECT LEVELS IN PURE CuInSe₂

Hall effect measurements of the temperature-dependent majority carrier concentration allow deeper insight into the activation energies of the dominant defects responsible for doping the CuInSe₂ thin films. Figures 5 and 6 show the electron concentration n and Hall mobility μ_H measured for four different n-type absorbers with copper-to-indium partial pressure ratios of $p_{Cu}/p_{In} = 0.70, 0.76, 0.90$, and 1.01, respectively, as a function of inverse temperature $1000/T$. Also shown is the hole concentration p and Hall mobility μ_H of the p-type absorber grown with $p_{Cu}/p_{In} = 1.2$ (open diamonds). The selenium supply of $p_{Se}/(p_{Cu} + p_{In}) = 26$ is constant for all samples. Solid lines in Figs. 5 and 6 are calculated numerically as described later.

For all n-type absorbers we measure significant electron densities even at low temperatures, comparable with previous results on nearly stoichiometric single crystals.[7] Even if we assume a very shallow donor, the electron concentration in the conduction band at lower temperature is expected to decrease stronger than that observed experimentally, largely due to the $T^{3/2}$ dependence of the effective density of states N_C at the conduction band edge, which is depicted by the dashed gray line in Fig. 5 (for the assumed material parameters see Table I). Hence, none of the n-doped samples shown in Fig. 5 can be adequately modeled assuming only band conductivity in a non-degenerate semiconductor, and the
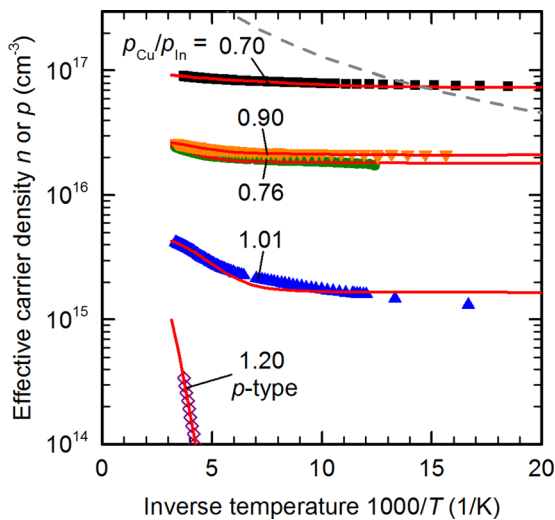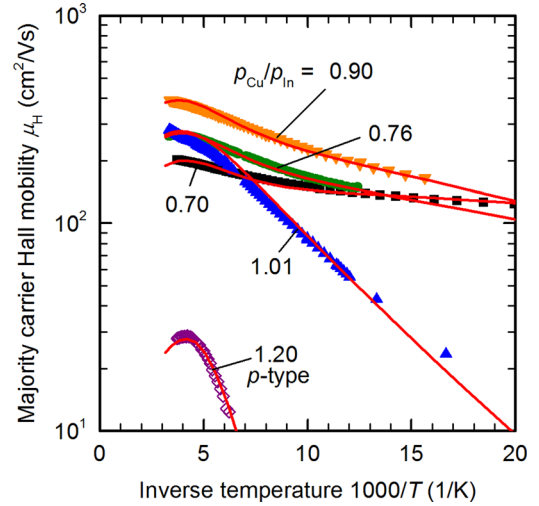

FIG. 6. Temperature dependent electron (solid symbols) and hole (open diamonds) Hall mobility as a function of inverse temperature $1000/T$ for a series of absorbers grown with different copper supplies. Solid lines are best fits to the data.

slope of $\ln(n)$ versus $1/T$ cannot be used to extract the defect activation energy.

All but the highest doped n-type absorbers furthermore show thermally activated mobilities with activation energies around 3–20 meV at low temperatures, which suggests that hopping conduction might play a significant role in these samples. For the highest doped absorber, the measured electron density at low temperatures is in fact even higher than the effective density of states N_C at the conduction band edge, which is a strong indication of the formation of a defect band. Accordingly, the mobility does not appear thermally activated as the electrons can move freely in the defect band, and the low-temperature mobility saturates to this defect band mobility. For higher p_{Cu}/p_{In} precursor partial pressure ratios, the electron mobility does not appear to saturate within the observed temperature range, presumably indicating defect concentrations slightly below the impurity band transition. The Mott criterion that defects with a concentration N_D form a defect band is given by[22]

$$N_D > \left[\frac{0.3}{a_0} \frac{\varepsilon_r}{m^*} \right]^3, \qquad (1)$$

where $a_0 \approx 52.9$ pm is the hydrogen Bohr radius, ε_r is the relative dielectric permittivity, and m^* is the effective mass of the carriers in the respective band in units of the free electron mass. For n-type CuInSe₂ ($\varepsilon_r = 13.6$, $m^* = 0.09$, Table I)

FIG. 5. Temperature-dependent effective electron (solid symbols) and hole (diamonds) concentration as a function of inverse temperature $1000/T$ for a series of absorbers grown with different copper supplies. Solid lines are best fits to the data, including quasi-free carriers in the bands and, for the n-type samples, an increased number of carriers due to hopping conduction. The dashed gray line corresponds to the effective density of states at the conduction band edge of CuInSe₂.

TABLE I. Material parameters assumed in our simulation according to Ref. 7 and references therein.

Effective mass m^*	0.09 (electron)
	0.73 (hole)
Dielectric constant ε	ε_r: 13.6 (static)
	ε_∞: 8.1 (high freq.)
Density ρ	5.77 g/cm³
Velocity of sound v_s	2180 m/s
Optical phonon temperature Θ	395 K

this relation yields $N_D > 5 \times 10^{16} \text{cm}^{-3}$, although the transition is expected to occur at considerably higher concentrations for compensated samples.[22] This range of defect concentrations is consistent with our results [compare with the extracted donor concentrations $> 10^{17} \text{cm}^{-3}$ shown in Fig. 7(a) and described later], which suggests that we indeed observe the transition to a delocalized defect band at low copper content.

In order to disentangle the different transport mechanisms and different dopant defects, we numerically model the temperature-dependent majority carrier concentration and Hall mobility for all samples. In order to compare our simulations with the experimental data obtained from Hall measurements, we combine band conduction and hopping conduction using a two-carrier model of the Hall effect, which yields

$$n_{eff} = \frac{(n_b \mu_b + n_d \mu_d)^2}{n_b \mu_b^2 + n_d \mu_d^2} \quad \text{and} \quad (2)$$

$$\mu_{eff} = \frac{n_b \mu_b^2 + n_d \mu_d^2}{n_b \mu_b + n_d \mu_d}, \quad (3)$$

where the subscript "b" denotes band conduction and "d" denotes conduction in the defect state, e.g., hopping or transport in a defect band. We fit the carrier density and mobility at the same time to derive a consistent set of defects describing both quantities with the same parameters.

The electron and hole densities in the conduction and valence bands are calculated from the Fermi level obtained by self-consistently solving the charge neutrality condition in the semiconductor for a given set of defects. Due to the shallow defect levels encountered in this study, we use a

numerical approximation to the Fermi-Dirac integral[23] in a parabolic band approximation instead of the commonly employed Boltzmann approximation. We include defect conduction by taking into account an electron concentration $n_d = f(E_F)N_{D1}$, where $f(E_F)$ is the probability that one of the shallowest donor states N_{D1} is occupied by an electron.

The band conduction mobility μ_b for electrons in the conduction band is calculated taking into account ionized[24] and neutral[25] impurity scattering, where we treat the occupied and empty defects as neutral or ionized impurities, respectively, as well as acoustic[26] and polar optical phonon scattering.[7] In accordance with Ref. 7 we neglect non-polar optical phonon scattering[27] for the *n*-type samples. The acoustic deformation potential is adapted for each sample to fit the high-temperature plateau of the effective mobility. The mobility for defect conduction is assumed to be of the form $\mu_d = \mu_0 \exp(-E_a/k_B T)$, with μ_0 and E_a as free parameters. Despite a possible influence from the surface roughness suggested by Fig. 4, we assume that the measured carrier mobility is indicative of the true bulk mobility.

We vary the activation energies and concentrations of two different donor states and one acceptor state, and the activation energy and pre-factor of the hopping mobility, to best reproduce the experimental data. The best fits are shown as red solid lines in Figs. 5 and 6. The material parameters assumed in the simulation are summarized in Table I, and sample-specific defect parameters are shown in Fig. 7 and Table II. It is apparent that we observe quite a spread in the acoustic deformation potential in the range of 23–42 eV. On the one hand it has been stated previously that the deformation potential is not constant in *n*-type CuInSe$_2$.[7] On the other hand, surface scattering or other effects not included in our simulation might reduce the maximum mobility at high temperatures, which in our simulation is dominated by phonon scattering, and we would thus obtain an erroneous value for the deformation potential. This also has a small effect on the degree of compensation, and hence the concentrations of the shallowest donor and the compensating acceptor, which is predominantly determined by the band mobility of the majority carriers due to its dependence on the total number of ionized defects. Nevertheless, we estimate this effect to influence the compensation ratio by less than 5%.

Figure 7(a) shows the dopant concentrations N_D of two donors and one acceptor, which are found to best describe
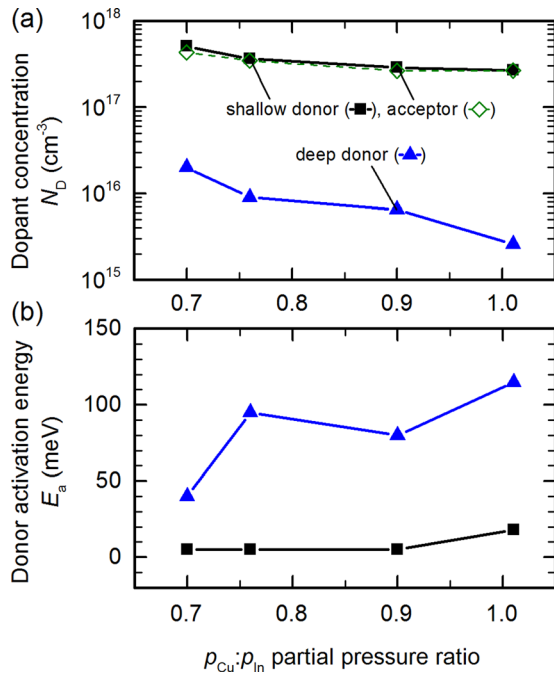

FIG. 7. (a) Dopant concentrations N_D of the shallow and deep donors (solid symbols) and compensating acceptors (open green diamonds), and (b) corresponding activation energies E_a of the donor states as a function of precursor partial pressure ratio p_{Cu}/p_{In} for *n*-type absorbers.

TABLE II. Sample-specific parameters obtained from a best fit to the experimental carrier concentration and mobility. Acoustic (E_{ac}) and non-polar optical (E_{npo}) deformation potentials, pre-factor μ_0 and activation energy E_a of defect conduction, and compensation ratio N_A/N_D for the *n*-type samples. For the *p*-type sample, the parameters of a transport barrier are given instead of defect conduction.

Sample, p_{Cu}/p_{In}	E_{ac} (eV)/E_{npo} (eV)	Hopping μ_0 (cm^2/V s)	Hopping E_a (meV)	N_A/N_D
0.70 (*n*)	42/—	325	1.5	0.82
0.76 (*n*)	33/—	270	4	0.93
0.90 (*n*)	23/—	420	5	0.90
1.01 (*n*)	35/—	500	18	0.98
1.2 (*p*)	3/7	(5500)	(80)	?

the experimental data as a function of the p_{Cu}/p_{In} precursor partial pressure ratio. For all samples, the concentration of the shallow donor is comparable in magnitude with the concentration of compensating acceptors, and hence all samples are highly compensated. Due to the resulting almost complete ionization of the shallow donors even at low temperatures, the deeper donor state also significantly contributes to the room-temperature carrier concentration of the films despite its comparably low concentration. All defect concentrations shown in Fig. 7(a), donors and acceptors, emulate the trend of the decreasing net electron concentration with higher Cu supply p_{Cu}/p_{In} as shown in Fig. 2(b). This leads to the conclusion that all the dominant dopant species for pure CuInSe$_2$ are determined by the Cu deficiency in the growth environment.

Figure 7(b) shows the activation energies of the shallow and deep donors. When taking into account only the simulated effective electron concentration, the simulation is not very sensitive to the activation energy of the shallow donor. This is due to the fact that this donor always contributes a charge carrier, either as an electron in the conduction band (ionized donor) or via defect conduction (neutral donor). We observe, however, that the activation energy must be close (within a few meV) to the activation energy E_a of hopping conduction in order to describe both electron concentration and mobility with the same set of defects. Hence, the experimental mobility provides a tight constraint on the activation energy of the shallow donor, and we obtain values of a few meV for most samples. Only the sample grown with $p_{Cu}/p_{In} = 1.01$ shows a different qualitative behavior and yields a significantly higher activation energy close to 20 meV.

The close relation between the activation energies of the shallowest donor state and of defect conduction indicate that hopping between two defects most likely occurs via thermal excitation to the conduction band. Hence, it is reasonable to identify the activation energy of the hopping mobility with the dopant activation energy. Indeed, the activation energies of 3–20 meV are consistent with a shallow donor commonly observed in CuInSe$_2$,[1,7] and agree well with the theoretical prediction of 7 meV obtained from the Hydrogen model with $\varepsilon_r = 13.6$ and $m^* = 0.09$ for a shallow donor in *n*-type CuInSe$_2$. This again supports our initial assumption that only the most shallow donor level contributes to the hopping conduction.

Further evidence for thermally activated transport in a defect band or via excitation to the conduction band is provided by the magnetoresistance of the *n*-type samples under investigation. The magnetoresistance $MR = [\rho(B) - \rho_0]/\rho_0$ for temperatures above 50 K and a magnetic field of $B = 7$ T remains below 2% for all samples, which implies that current is predominantly carried by charge carriers of the same polarity and with similar transport properties. In the transition range from band to defect conduction this requires that the corresponding mobilities of electrons in the conduction band and in the defects are of similar magnitude; otherwise, we would observe a maximum in magnetoresistance and a corresponding minimum in effective electron concentration. Such high mobilities (>100 cm^2/Vs) are however unexpected for direct hopping processes between separate defects over long

distances, which again suggests excitation to a delocalized state. For the sample grown with $p_{Cu}/p_{In} = 1.01$, where we have recorded the magnetic-field-dependent resistivity for temperatures down to 15 K, we in fact observe a pronounced positive magnetoresistance at temperatures well below 50 K. At a magnetic field of $B = 7$ T we obtain a magnetoresistance of 10% at 30 K, which increases to 60% at 15 K. Hence, at low temperatures, distinctly different charge carriers contribute significantly to the current, which might indicate that thermal excitation of electrons to a delocalized state is no longer efficient at low temperatures, especially for the fairly high activation energy close to 20 meV of this particular sample.

For the deep donor state shown in Fig. 7, the activation energy increases with higher Cu supply, while the defect concentration decreases. Qualitatively, such a reduced thermal activation energy for high defect concentrations has indeed been observed for many semiconductors.[28] For a precise quantitative analysis, however, the number of datapoints available for the deep donor state in Fig. 7 is insufficient.

Although we do not discuss this sample in detail, we have included simulations on the nearly stoichiometric *p*-type sample. Unlike for the *n*-type samples, the thermally activated hole mobility cannot be explained by defect conduction due to the exponentially decreasing hole concentration, but must instead be caused by a transport barrier. As discussed earlier in relation to the EDX analysis, we observe patches of a secondary phase on this particular sample, which might impede current flow due to lateral variation in electronic properties. Accordingly, the mobility is not only affected by phonon and impurity scattering, and we cannot obtain the total defect concentration from our fit. We obtain a deep acceptor with an activation energy around 170 meV, which is fairly deep compared with values of 40 and 60 meV commonly observed.[1] Note, however, that we would be unable to resolve more shallow acceptors if they were completely compensated by donors. The trends of the donor and acceptor concentrations obtained from the *n*-type samples in this study, i.e., a compensation ratio $N_A/N_D \rightarrow 1$ near stoichiometry, suggest that this might indeed be the case.

The experimental results presented in this section alone do not allow to identify the atomistic nature of the defects involved. Nevertheless, comparison with theoretical predictions of point defect levels allows to identify the most likely candidates for each dopant defect, taking into account the observed trend of defect properties with varying copper supply. Recent numerical calculations of point defects in CuInSe$_2$ by several groups[29–31] agree on the dominant shallow donor (In$_{Cu}$ antisite, Cu$_i$ and In$_i$ interstitials, V$_{Se}$ vacancy) and acceptor (V$_{Cu}$ and V$_{In}$ vacancies, Cu$_{In}$ interstitial) species. The In-on-Cu antisite defect (In$_{Cu}$) is identified as a shallow donor and considered to be dominantly responsible for the strong *n*-type doping in Cu-poor CuInSe$_2$[29,32] due to its low formation enthalpy. Hence, we propose In$_{Cu}$ defects to be the origin of the dominant shallow donor observed in this study. In agreement with the dopant concentrations shown in Fig. 7(a), their concentration would be expected to increase under increasingly Cu-poor growth conditions. Possible candidates for the deep donor are interstitial Cu$_i$ and In$_i$, as well as

Se vacancies (V_{Se}). Due to their comparably high formation enthalpy, these defects will be formed in considerably smaller numbers compared with In_{Cu}, consistent with the lower concentration of the deeper donor shown in Fig. 7(a). For interstitial Cu_i, however, the concentration would be expected to decrease—opposite to the trend of the donor concentration—for a reduced Cu supply during film growth, which likely rules out Cu_i as the origin of the deep donor. Of the remaining two candidates, we consider V_{Se} to be the most likely origin of the deep donor due to the significantly higher formation enthalpy of In_i.

Regarding acceptors, the three different acceptor levels commonly observed in $CuInSe_2$ can be attributed to V_{Cu}, Cu_{In}, and V_{In} defects, in order of increasing energetic distance from the valence band edge.[29–31] Due to their full ionization we cannot obtain the acceptor activation energies from our measurements on *n*-type $CuInSe_2$. The trend of decreasing acceptor concentration with increasing Cu content in the film observed in Fig. 7(a) however suggests that at least some fraction of all acceptors is indeed related to Cu vacancies.

Our proposed attribution of the observed defect levels to intrinsic point defects is in agreement with neutron powder diffraction experiments by Stephan *et al.*,[32] where they find large concentrations of V_{Cu}, Cu_{In}, and In_{Cu} in Cu-poor $CuInSe_2$ powder samples. Note that they have only addressed cation defects, and hence any V_{Se} present would not be detected. It is worth noting that our observation of *n*-type doping for Cu:In > 0.9 is in contradiction to predictions of the doping polarity given in the same study by Stephan *et al.*[32] based on their experimentally determined cation defect densities, where they assume spontaneous formation of electrically inactive defect pairs according to calculations by Zhang *et al.*[33,34] This deviation, however, could simply be due to differences in absolute defect concentration between our and their samples, due to the additional influence of anion defects, or due to the neglect of defect kinetics as discussed in Ref. 31.

V. THE INFLUENCE OF SODIUM ON DOPING

In Secs. III–IV, we have shown that as-grown Cu-poor pure $CuInSe_2$ samples are always *n*-type. Polycrystalline Cu-poor $CuInSe_2$ or $Cu(In,Ga)Se_2$ solar cell absorbers, on the other hand, are always *p*-type; otherwise, the solar cell would not work as intended. One major difference between polycrystalline and epitaxial absorbers is the choice of substrate material. While our epitaxial samples are grown on high-purity sodium-free GaAs wafers, polycrystalline absorbers for solar cell fabrication are typically deposited onto soda-lime glass, which contains high amounts of sodium (Na). Although nominally Na-free glass substrates, foils, or dielectric Na-blocking layers might be used to minimize Na incorporation, trace amounts of Na might still be present in the materials or in the deposition chamber from previous runs.[35] We propose that Na diffusing into the absorber during absorber formation might be responsible for the *p*-doping commonly observed for polycrystalline Cu-poor $CuInSe_2$. In fact, Na is known to increase the net *p*-doping in *p*-type

$CuInSe_2$ devices by influencing the native defect chemistry.[10–15]

Therefore, we investigate the influence of Na on the electrical properties of $CuInSe_2$ by incorporating Na into the epitaxial (i.e., single crystal) pure $CuInSe_2$ in a gas-phase post-deposition treatment involving no elements other than Na and Se. Prior to the first post deposition treatment, a thorough cleaning of the furnace assembly (consisting of new components: quartz tubes and graphite parts) was performed by flushing with running $18.2\,M\Omega\,cm$ deionized water and push-drying the excess water with a nitrogen flux. Reasonable measures were taken to ensure manipulation under minimized risk of Na contamination by using rinsed gloves, tools, and accessories. The furnace was then heated under constant vacuum ($<10^{-2}\,mbar$) to $800\,^{\circ}C$ for $48\,h$, before allowing a natural cool down to room temperature. For this experiment we have chosen a sample with Cu:In $= 0.89$ [grown with $p_{Se}/(p_{Cu} + p_{In}) = 26$ and $p_{Cu}/p_{In} = 0.7$], which initially showed the highest electron concentration among the chalcopyrite samples analyzed in this study. The sample was broken into stripes $5\,mm$ wide and a few centimeters long, which allowed to process different Hall specimens from the same sample, corresponding to different distances from the Na source. In the first run, a piece of the sample is placed in the clean assembly, together with a reservoir of elemental selenium to replace possible selenium loss, and annealed in a nitrogen ambient at a temperature of $570\,^{\circ}C$ for $30\,min$. Note that no intentional Na was present in this run. In the second run, Na_2Se salt is added to the selenium reservoir in the graphite box, and a fresh piece of the same sample is annealed with the same process. As a reference, we kept a piece of the sample without any post-deposition treatment.

Secondary ion mass spectrometry (SIMS) was performed at several spots on the samples in order to verify Na incorporation into the film. In addition to Na incorporation, we observe a Ga diffusion from the substrate wafers into the $CuInSe_2$ films upon annealing. We find that the sum of the Ga and In signals is virtually constant throughout the film, and that the In signal extends deeper into the GaAs substrate wafer for films with a more pronounced Ga diffusion. This suggests that Ga replaces In and is indeed incorporated into the $CuInSe_2$ films. Further discussion of the enhanced In/Ga interdiffusion by sodium is beyond the scope of this study and will be presented in a separate manuscript.

Figure 8 shows SIMS depth profiles of the relative gallium content, GGI = [Ga]:([Ga] + [In]), and the relative sodium intensity for the three different samples at different distances from the Se and Na_2Se reservoir. In the case of the Na-treated sample, the close proximity to the Na source led to the formation of multiple cracks and Na-containing clusters near the sample edge, and we have hence discarded these results. Although we expected both untreated and Se-treated reference samples to be free of Na, we detect small amounts of Na in both samples, possibly due to trace amounts of Na in the Se used for the experiment and in the MOVPE growth chamber or precursor chemicals. For a given sample we observe slightly increased Na and Ga concentrations closer to the Se and Na_2Se source. Furthermore, the Na-treated
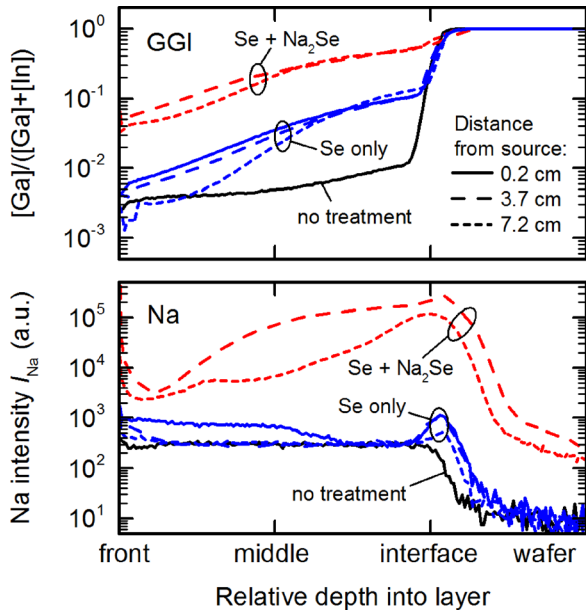
FIG. 8. SIMS depth profile of GGI [atomic ratio of Ga:(Ga + In), top part] and Na (bottom part) for an untreated sample (black line), the nominally "Na-free" Se-treated sample (blue lines), and a Na-treated sample (red lines) at different distances from the Se and Na$_2$Se source. The profile closest to the Na source for the Na-treated sample is omitted due to severe cracking and cluster formation.

sample consistently shows the highest Ga content of the three different samples. Accordingly, the Ga incorporation appears to correlate with the amount of Na present in the films after treatment, and further investigation will be necessary to decouple the effect of Na and Ga on the electrical parameters.

We again employ Hall measurements to investigate the electrical properties of the treated films. However, the nominally "Na-free" Se-treated sample shows an extremely high resistivity of the order of 10^3–$10^4 \, \Omega \, cm$, compared with $0.3 \, \Omega \, cm$ for the untreated reference and $250 \, \Omega \, cm$ for the Na-treated sample, and we were unable to obtain meaningful results from the Hall measurements. In a first attempt to disentangle the influence of Na and Ga on the electrical properties, we grew a Cu-poor epitaxial Cu(In,Ga)Se$_2$ film with a nominal GGI = 0.06 (actual GGI = 0.04–0.07 determined by SIMS throughout the depth of the film) by partly replacing the Trimethyl-indium flow by Triethyl-gallium, leaving all other growth parameters unchanged from the original Ga-free CuInSe$_2$ process used for this Na-doping experiment. Note that we are limited to fairly low Ga contents without changing the growth process parameters. Despite the added Ga we do not observe any significant changes in carrier concentration, and particularly we still obtain n-type films with a resistivity of $0.3 \, \Omega \, cm$. Hence it appears unlikely that the observed significant changes in the electrical properties after Se-treatment are caused by Ga incorporation. Annealing in Se ambient might have reduced the net doping due to a reduced concentration of V_{Se}-related donors. This interpretation however is at odds with our attribution of the dominant donor to In$_{Cu}$ antisites, as discussed in Section IV. Instead, two different mechanisms might be responsible for the increased resistivity: Although the Na concentration after

Se-treatment is similar to the untreated reference, a slightly higher amount of Na present might have been just enough to reduce the net doping to a nearly intrinsic level. This would explain the high resistivity of the treated film and highlights the sensitivity of the absorber doping to even minute amounts of Na. Alternatively, the high-temperature treatment might allow reactions of mobile defect species and the dissociation of defect pairs.[31]

After the Na treatment, the film is p-type with a free hole concentration at 270 K of the order of $p \approx 10^{15} \, cm^{-3}$. A fit to the temperature-dependent hole density yields an acceptor state with an activation energy of approximately 60 meV and an acceptor concentration of the order of $N_A \approx 10^{17} \, cm^{-3}$, and a comparable concentration of compensating donors of $N_D \approx 10^{17} \, cm^{-3}$, $N_D < N_A$. Note, that for the Na-treated samples we cannot use the measured hole mobility to estimate the total defect density, as discussed later. Hence, further shallow acceptor states might be present in the absorber—together with a comparable density of compensating donors—without being resolved in the measurement due to their full compensation. Nevertheless, we can conclude that the Na-doped sample is highly compensated with $N_D/N_A > 0.9$.

Unlike the untreated samples analyzed in this study, the Na-treated films are highly resistive due to a significantly reduced hole mobility of $3 \, cm^2/Vs$ at $T = 270 \, K$, which furthermore shows a thermally activated behavior with an activation energy of 30 meV. For monocrystalline CuInSe$_2$, such low mobility values cannot be theoretically reproduced using credible material parameters for band conduction. In particular, this difference cannot be solely ascribed to the higher effective mass of the holes compared with the electrons as majority carriers, neither to a larger concentration of point defects. We would obtain an erroneously low mobility if the films were not completely converted to p-type, i.e., if the front or rear surface of the film remained n-type. This is ruled out in our case due to a negligible magnetoresistance of $[\rho(B) - \rho_0]/\rho_0 < 2\%$ at $B = 7 \, T$. In polycrystalline material, however, Hall measurements are expected to severely underestimate the in-grain mobility due to the presence of grain boundaries.[36] Indeed, we observe a partial restructuring of the absorber surface and the appearance of small cracks upon Na doping, possibly leading to the formation of transport barriers across the absorber film, which could explain the low experimental mobility values.

VI. CONCLUSIONS

Epitaxial CuInSe$_2$ thin films were grown by MOVPE on sodium-free GaAs substrate wafers. The defect concentration and majority carrier mobility were analyzed over a wide range of growth conditions, varying the relative amount of copper, indium, and selenium present during growth. EDX analysis revealed that the films are already nearly stoichiometric in composition for slightly copper-poor growth conditions with a precursor partial pressure ratio of $p_{Cu}/p_{In} > 0.75$. Below that threshold, significant deviations from stoichiometry were resolved by EDX.

In contrast to common Cu-poor polycrystalline solar cell absorbers, all Cu-poor epitaxial absorbers were found to be

n-type. The electron concentration was shown to decrease with higher copper content in the films. For nearly stoichiometric samples with similar atomic copper-to-indium ratios in the films (grown with $p_{Cu}/p_{In} > 0.75$), the electron concentration also decreases with higher copper-to-indium partial pressure ratio p_{Cu}/p_{In}.

The temperature-dependent effective carrier concentration and mobility were obtained for a set of samples grown with different copper-to-indium partial pressure ratios. The electron concentration at low temperatures was shown to be very high and only weakly dependent on temperature, which was attributed to defect conduction in a shallow donor. This assumption was justified by the absence of notable magnetoresistance above temperatures of 50 K and a thermally activated electron mobility, which was attributed to indirect hopping between different defects via thermal excitation to delocalized states in the conduction band. Two different donor defects with activation energies around 3–20 meV and 40–120 meV were shown to describe the experimental data well, as long as defect conduction in the shallow donor is taken into account. All defect concentrations were shown to increase toward more Cu-poor growth conditions, indicating that the relevant dopant defects are related to the Cu deficiency in the growth process. The most likely origin of the strong *n*-type doping was proposed to be In$_{Cu}$ antisites (dominant shallow donor), and Se vacancies or In interstitials (deep donor).

Annealing the absorber in the presence of selenium and sodium changed the conductivity type from *n*-type (in this experiment initially $n \approx 10^{17}$ cm^{-3}) to *p*-type ($p \approx 10^{15}$ cm^{-3} at $T = 270$ K). The presence of sodium furthermore appears to facilitate the diffusion of gallium from the GaAs substrate into the CuInSe$_2$ film, and further work is required to disentangle direct effects of Na incorporation and indirect effects of Na-induced Ga diffusion. Nevertheless, sodium impurities might be responsible for the *p*-type doping observed in polycrystalline solar cell absorbers, even if their composition is Cu-poor. It was proposed that defect reactions at elevated temperatures or trace amounts of sodium might significantly affect the electrical properties of the absorber. Accurate control of the thermal history and Na content is thus required for a meaningful comparison of the electrical properties of different Cu(In,Ga)Se$_2$ thin films.

ACKNOWLEDGMENTS

[1]S. Siebentritt, M. Igalson, C. Persson, and S. Lany, Prog. Photovoltaics: Res. Appl. **18**, 390–410 (2010).

[2]R. Noufi, R. Axton, C. Herrington, and S. K. Deb, Appl. Phys. Lett. **45**, 668–670 (1984).

[3]H. Neumann and R. D. Tomlinson, Sol. Cells **28**, 301–313 (1990).

[4]S. Nomura, J. Itoh, and T. Takizawa, Jpn. J. Appl. Phys., Part 1 **32**, 97–98 (1993).

[5]A. Mudryi, T. Tavrina, and E. Rogacheva, Inorg. Mater. **43**, 926–930 (2007).

[6]H.-J. Ko *et al.*, J. Cryst. Growth **322**, 91–94 (2011).

[7]S. M. Wasim, Sol. Cells **16**, 289–316 (1986).

[8]G. Hanna, J. Mattheis, V. Laptev, Y. Yamamoto, U. Rau, and H. Schock, Thin Solid Films **431–432**, 31–36 (2003).

[9]M. A. Contreras, I. Repins, W. K. Metzger, M. Romero, and D. Abou-Ras, Phys. Status Solidi A **206**, 1042–1048 (2009).

[10]L. Kronik, D. Cahen, and H. W. Schock, Adv. Mater. **10**, 31–36 (1998).

[11]D. J. Schroeder and A. A. Rockett, J. Appl. Phys. **82**, 4982–4985 (1997).

[12]W.-J. Tsai *et al.*, Thin Solid Films **519**, 1712–1716 (2010).

[13]R. Kimura *et al.*, Sol. Energy Mater. Sol. Cells **67**, 289–295 (2001).

[14]D. Rudmann *et al.*, Appl. Phys. Lett. **84**, 1129–1131 (2004).

[15]V. Deprédurand *et al.*, J. Appl. Phys. **115**, 044503 (2014).

[16]B. Tell, J. L. Shay, and H. M. Kasper, J. Appl. Phys. **43**, 2469–2470 (1972).

[17]S. Siebentritt, Thin Solid Films **403–404**, 1–8 (2002).

[18]N. Rega, S. Siebentritt, I. Beckers, J. Beckmann, J. Albert, and M. Lux-Steiner, J. Cryst. Growth **248**, 169–174 (2003).

[19]T. Gödecke, T. Haalboom, and F. Ernst, Z. Metallkd. **91**, 622–634 (2000).

[20]L. J. van der Pauw, Philips Tech. Rev. **20**, 220–224 (1958).

[21]R. Chwang, B. J. Smith, and C. R. Crowell, Solid-State Electron. **17**, 1217 (1974).

[22]N. F. Mott and J. H. Davies, Philos. Mag. B **42**, 845 (1980).

[23]W. B. Joyce and R. W. Dixon, Appl. Phys. Lett. **31**, 354–356 (1977).

[24]H. Brooks, Phys. Rev. **83**, 879 (1951).

[25]N. Sclar, Phys. Rev. **104**, 1559–1561 (1956).

[26]J. Bardeen and W. Shockley, Phys. Rev. **80**, 72–80 (1950).

[27]J. D. Wiley and M. DiDomenico, Phys. Rev. B **2**, 427–433 (1970).

[28]G. L. Pearson and J. Bardeen, Phys. Rev. **75**, 865–883 (1949).

[29]J. Bekaert, R. Saniz, B. Partoens, and D. Lamoen, Phys. Chem. Chem. Phys. **16**, 22299–22308 (2014).

[30]J. Pohl and K. Albe, Phys. Rev. B **87**, 245203 (2013).

[31]L. E. Oikkonen, M. G. Ganchenkova, A. P. Seitsonen, and R. M. Nieminen, J. Phys.: Condens. Matter **26**, 345501 (2014).

[32]C. Stephan, S. Schorr, M. Tovar, and H.-W. Schock, Appl. Phys. Lett. **98**, 091906 (2011).

[33]S. B. Zhang, S.-H. Wei, and A. Zunger, Phys. Rev. Lett. **78**, 4059–4062 (1997).

[34]S. B. Zhang, S.-H. Wei, A. Zunger, and H. Katayama-Yoshida, Phys. Rev. B **57**, 9642–9656 (1998).

[35]P. Dale, paper presented at the 25th EUPVSEC, Hamburg, Germany, 2015.

[36]J. Jerhot and V. Snejdar, Thin Solid Films **52**, 379–395 (1978).